CrossMark

Long-term monitoring of bottom environments of the continental slope off Otsuchi Bay, northeastern Japan

Kazumasa Oguri[1] · Yasuo Furushima[1] · Takashi Toyofuku[1] · Takafumi Kasaya[1] · Masahide Wakita[1] · Shuichi Watanabe[1] · Katsunori Fujikura[1] · Hiroshi Kitazato[1]

Abstract Long-term monitoring of the seafloor environment off Otsuchi Bay, northeastern Japan, was carried out to investigate environmental changes of the deep-sea floor after the 2011 off the Pacific coast of the Tohoku Earthquake. We deployed two deep-sea stations, one on an upper continental slope site (around 300 m water depth) and the other on a bathyal (998 m) site, to measure current intensity and direction, water temperature, salinity, dissolved oxygen, and turbidity, and to obtain seafloor images. The monitoring period on the upper slope was 9 months (March–September 2013), and 14 months (August 2012–October 2013) at the bathyal site. The oceanographic data from the upper slope site recorded the seasonal exchange of water masses and dense marine snowfall from April to May 2013. On 7 December 2012, a large aftershock of the 2011 earthquake caused increased turbidity at the bathyal site, and seafloor photographs and videos recorded the disturbance and recovery of benthic habitats. The data from these deployments show that long-term monitoring can provide important oceanographic, biological, and sedimentological data from deep-sea sites. Together with shipboard and deep-tow observations and data collected by remotely operated vehicles, long-term monitoring can be a valuable tool for understanding deep-sea environments and their variability.

✉ Kazumasa Oguri
  ogurik@jamstec.go.jp

[1] Japan Agency for Marine-Earth Science and Technology (JAMSTEC), 2-15 Natsushima-cho, Yokosuka, Kanagawa, 237-0061, Japan

1 Introduction

On 11 March 2011, the Tohoku Earthquake off the Pacific coast of Japan caused strong shaking and a huge tsunami along the entire Pacific coast of the Tohoku region of Japan. After the earthquake and many aftershocks, dense nepheloid layers were widely observed in the sea off northeastern Japan (Kawagucci et al. 2012; Noguchi et al. 2012; Oguri et al. 2013). Fine sediment with a high water content, presumably related to turbidity currents, widely covered the seafloor, in both shallow and hadal regions (Ikehara 2012; Ikehara et al. 2012; Oguri et al. 2013; Nomaki et al. 2015). Surface sediments (Arai et al. 2013) and meiobenthic habitats (Toyofuku et al. 2014) were disturbed not only by earthquake shaking but also by unusually intensive hydrodynamic currents triggered by the tsunami. Physical disturbances to the seafloor caused by the series of earthquakes and the tsunami were investigated during many cruises carried out just after the disaster. However, changes to the seafloor environments have not been fully explored because access to the seafloor has been limited. The northeastern Pacific coast and continental slope of Japan are characterized by high primary productivity, owing to the mixing of warm and cold water systems (Saino et al. 1998), and fisheries are quite active. In 2010, for example, 97,857 tonnes of fish were caught by the fisheries of Iwate Prefecture (Iwate Prefecture 2011). When the area of coseismic slip is taken into account (Ozawa et al. 2011; Sato et al. 2011), physical disturbances to the seafloor resulting from the earthquake are likely to have influenced fisheries throughout

the northeastern region. To document and understand the seafloor environments and changes caused by the seismic disturbance, we deployed two deep-sea stations for long-term monitoring, one on the upper slope of the continental shelf and the other lower on the slope off Otsuchi Bay in the Sanriku region of northeastern Japan. Here, we report the results during this monitoring period and the environmental variability observed in the temperature, salinity, dissolved oxygen concentration (DO), and turbidity data. Time-lapse photography of the seafloor also recorded the characteristics of the sediments and benthic habitats at the two sites.

2 Methods

2.1 Seafloor monitoring and CTD sites

Two seafloor deployment sites were selected for environmental monitoring, one at approximately 300 m water depth on the continental shelf (upper slope site), and the other at 998 m depth on the slope (bathyal site) (Fig. 1; Table 1). Both sites are at about the same latitude (~39°20′N). The upper slope site is in an active fishery area, and trawling is frequently conducted around its water depth, except between July and August. The bathyal site is within the O_2-depleted zone of the North Pacific (DO < 45 μM; found at water depths from 700 to 1300 m; Ogura 1970; Fontanier et al. 2014). Although there is little fishery activity at the bathyal depth, some important fishery resources such as *Sebastolobus macrochir* is distributed at that depth (e.g., Hattori et al. 2007; Sakaguchi-Orui et al. 2014), and knowledge of benthic habitats is essential information for understanding the ecology of such fish. It is also important to observe environmental parameters at this depth to understand how intermediate waters change seasonally at the seafloor, because these variations have not been well understood.

We deployed one deep-sea station at the bathyal site on 14 August 2012, during cruise YK12-10 of R/V *Yokosuka*
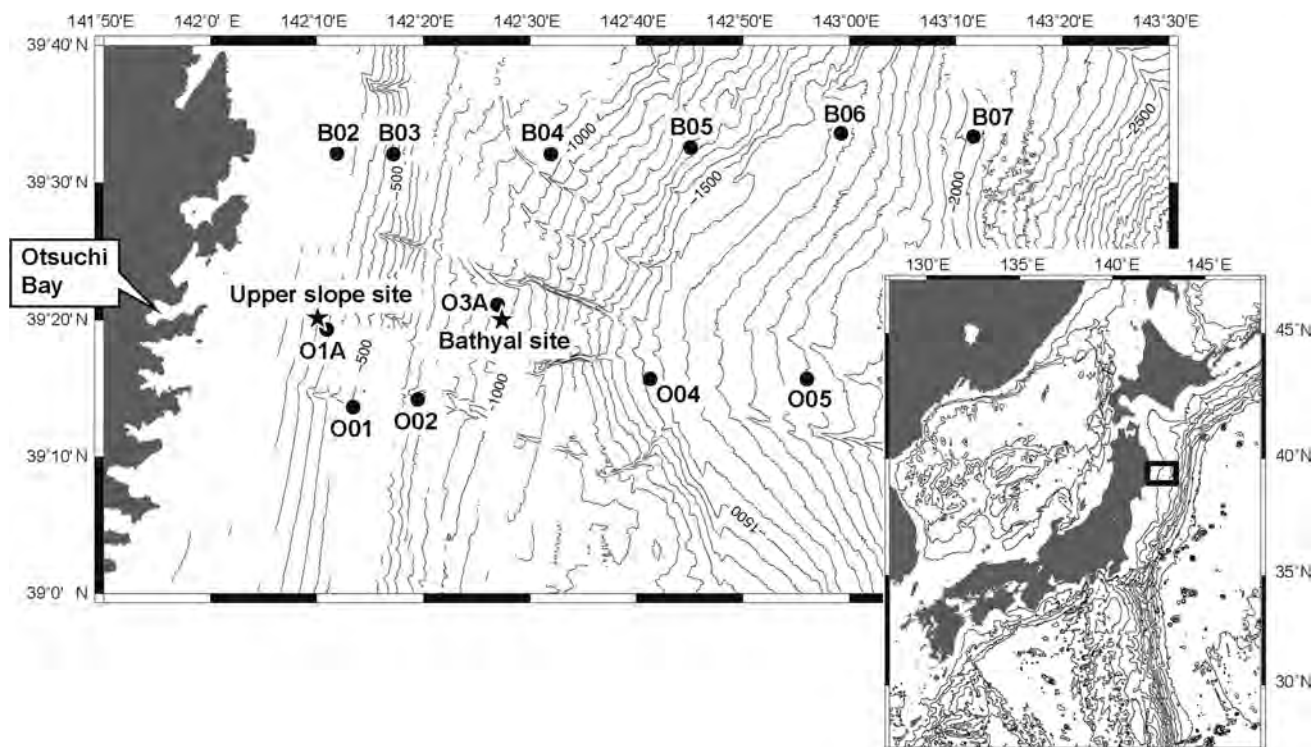

Fig. 1 Long-term monitoring sites on the seafloor (*stars*) and CTD sites where measurements were obtained during the BO13-20 cruise (*solid circles*) off Otsuchi Bay, Sanriku region. The isobath interval is 50 m. On the wide area map (*inset*; isobath interval, 1000 m), the *rectangle* shows the location of the mapped area in relation to the Japanese islands

Table 1 Locations and water depths of the two monitoring sites and the deployment periods

Site	Latitude (N)	Longitude (E)	Initial water depth (m)	Deployed periods
Upper slope	39°19.981′	142°09.994′	300	13 Mar 2013–2 Sep 2013
Bathyal	39°19.978′	142°27.519′	998	14 Aug 2012–14 Oct 2013

(JAMSTEC), and a second station at the upper slope site on 12 March 2013, during the R/V *Dai 18 Kaiko-Maru* cruise (Offshore Operation). The station deployed at the bathyal site was recovered on 14 October 2013 during leg 1 of the NT13-21 cruise of R/V *Natsushima* (JAMSTEC). The station deployed at the upper slope site was unintentionally picked up by a fishing trawler on 3 September 2013. After its unexpected recovery, the station was kept in storage in port. The measuring instruments were hermetically sealed and all data and photos were recovered safely.

To further investigate the water mass distributions off Otsuchi Bay, CTD (conductivity, temperature and depth sensors; SBE 9plus, Sea-Bird Electronics) observations were conducted between 28 October and 10 November 2013 during cruise BO13-20 of R/V *Bosei-Maru* (Tokai University) (Fig. 1). Seawater samples were also collected into 10-L Niskin bottles. Then, the salinity was measured with a Model 8400B "Autosal" salinometer (Guildline Instruments; S/N 6286). The CTD data were calibrated against the salinity data.

2.2 Deep-sea stations, sensors, and cameras

The two stations were designed for long-term monitoring of the seafloor environment (Fig. 2). Their design was based on the concept of a benthic lander (Smith et al. 1976), which was made to be released from a ship for analyses of benthic processes on the seafloor below (e.g., Tengberg et al. 1995). The frames were constructed with titanium pipes to prevent corrosion during long-term deployments. For environmental monitoring, an acoustic Doppler current profiler (ADCP) equipped with temperature, conductivity, DO, turbidity, and hydrostatic pressure sensors (RDCP 600 with 4050, 4019B, 3830, 3612A, and 4017D sensors, respectively; Xyrem) was mounted on the frame. The monitoring interval of the RDCP 600 and the attached sensors was set to 1 h. A camera system was also mounted on the side of the frame to record time-lapse changes of the seafloor environment and benthic habitats. With this system, a photograph was taken daily, and, at the bathyal site only, a video was recorded weekly, during the deployments. Total time of each video sequence was 4 min 35 s. This camera system consisted of a HDTV camera (GZ-V570 modified; JVC Kenwood) and a custom-made low-power consumption timer circuit combined with a microprocessor (PIC18F14K50; Microchip Technologies) and a real-time clock module (RTC-8564NB; EPSON Toyocom). The photographic resolution was 3800 × 2856 pixels and 1920 × 1080 pixels at the upper slope and bathyal sites, respectively. The pixel size of the video recordings at the bathyal site was also 1920 × 1080 pixels. The camera was
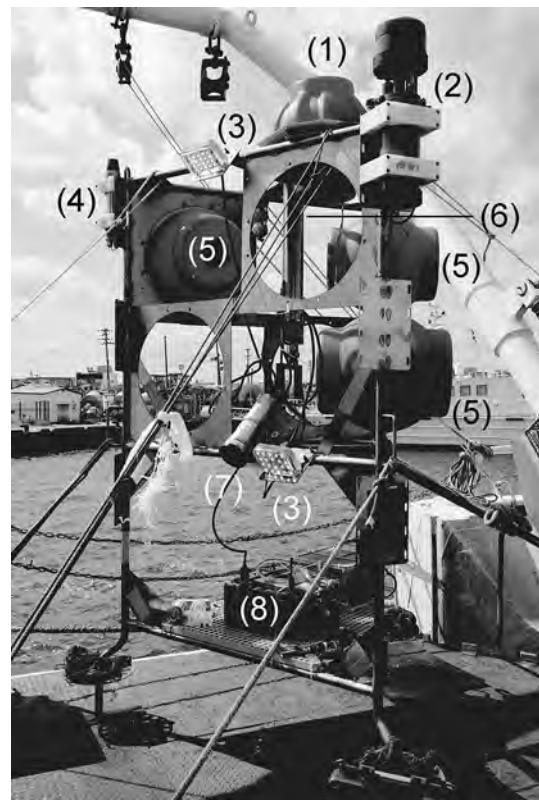

Fig. 2 A deep-sea station used for the monitoring. The frame is constructed with titanium pipes. The installed instruments are *1* ARGOS satellite transmitter, *2* RDCP 600, ADCP-CTDDO-turbidity sensors with battery, *3* LED lights, *4* ROV homer, *5* glass spheres, *6* acoustic release transponder, *7* HDTV camera in a SUS316 stainless pressure cylinder, and *8* oil-filled lithium ion battery to supply power to the camera and lights

mounted on the frame at 1 m height above the sea floor. A trapezoidal area of the seafloor was photographed with a transversal line of 115 cm and a vertical line of 50 cm (Yamakita, personal communication). Two LED lights plasticized in epoxy resin blocks (custom-made; Oguri et al. 2015) were also mounted on the frame. The camera and the lights were automatically switched on during photography following the sequence as programmed in the timer circuit. Electronic power for the sensors and the camera systems was supplied by 14.4 V lithium ion battery (capacity of 40 Ah), installed in an insulated oil-filled enclosure to compensate for the pressure.

Two different acoustic transponders were also installed on the frame. An acoustic release transponder (TMR-6005B; Kaiyo Denshi) transmitted to the ship the approximate deployment site when the station was deployed, and an ROV-Homer (Model 7382; Sonardyne) allowed the station to be located for recovery by a remotely operated vehicle (ROV).

2.3 Sensor configurations

2.3.1 Salinity calculation

Salinity data were calculated from conductivity values by using the RDCP studio software bundled with the RDCP 600. Because we used the induction-based conductivity sensors, the metal frame can affect the sensor reading. To obtain precise salinity values, we compared the temperature and salinity obtained from the station data with data obtained during the BO13-20 cruise. The measured salinity was 0.75 lower at the upper slope site, and 0.35 lower at bathyal site, than the reference values. The salinity data were corrected by adding these offsets. No correction was used for the temperature data.

2.3.2 Compensation of the O_2 sensor

The DO values from the 3830 optode sensor are influenced by temperature, salinity, and hydrostatic pressure. We used the following equation to obtain actual DO values from the raw data (Aanderaa Data Instruments 2003; Uchida et al. 2008):

$$[O_{2\text{corr}}] = [O_{2\text{raw}}] \times e^{\left\{ S \cdot \left(B_0 + B_1 \cdot t + B_2 \cdot t^2 + B_3 \cdot t^3 \right) + C_0 \cdot S^2 \right\}}$$
$$\times \left(1 + \frac{0.032 \times d}{1000} \right),$$

where $(O_{2\text{corr}})$ is corrected DO in μM, $(O_{2\text{raw}})$ is the raw O_2 value from the optode sensor, B_0–B_3 and C_0 are constants representing the sensor foil characteristics shown in the operating manual, S is salinity, t is temperature (°C), and d is depth (m) or hydrostatic pressure (dbar). To obtain $(O_{2\text{corr}})$ values, corresponding salinity, temperature and hydrostatic pressure data from the respective sensors were substituted into the equation.

The data of the DO sensor deployed at the upper slope site showed a decreasing trend. From two temperature-compensated O_2 values obtained under the close atmospheric pressure measured before and after the deployment (343 μM at 1019.9 hPa, at 08:40 JST on 12 March 2103 and 282 μM at 1019.8 hPa, at 04:40 JST on 7 September 2013; Miyako Meteorological Observatory, Japan Meteorological Agency), the calculated rate was −0.0142 μM h^{-1}. This rate was used to correct DO values at the upper slope site. There was no decreasing trend in the bathyal site data.

2.3.3 Adjustment of the internal compass of the ADCP sensor

Prior to the deployment, the internal compass of the ADCP sensor was adjusted for the magnetic declination of −7°26′

(Geospatial Information Authority of Japan 2010). By this adjustment, the current direction data were corrected to the accurate azimuth.

2.3.4 Offset adjustment of the turbidity sensors

The turbidity sensor of the RDCP 600 had an initial offset. We determined the offset value by measuring turbidity in the dark on board the ship. The offset was –0.09 NTU at the upper slope site and 0.625 NTU at the bathyal site. These values were then subtracted from the observed values at the respective sites.

3 Results

3.1 Data overview

At the upper slope site, 4201 measurements of each parameter were recorded (water temperature, salinity, DO, hydrostatic pressure, and current direction and intensity). The camera captured 175 seafloor photographs. At the bathyal site, 10222 measurements of each parameter were recorded, and the camera captured 187 photographs and 61 HDTV videos.

3.2 Hydrostatic pressure and pitch and roll at the upper slope site

At the upper slope site, the recorded hydrostatic pressure showed clear changes during the deployment. The initial pressure of 3027.1 kPa increased to 3105.3 kPa at 04:38 on 15 March, and at 9:38 on 17 March, it decreased to 2870.9 kPa. At 06:38 on 17 March, it decreased markedly to 2656.1 kPa (Fig. 3a). By assuming an average seawater density in the water column of 1.026, the water depths on these dates were estimated to be 295, 303, 280, and 259 m.

These depth changes suggest that the station was dragged about, perhaps as a result of nearby trawling. Furthermore, even though the pressure remained constant from 17 March to 30 May, both pitch and roll angles changed four times (at 08:38 on 26 March, at 20:38 on March 28, at 10:38 on 3 March and at 00:38 on 5 May, see Fig. 3a), suggesting that the station frame was buffeted about by trawling during this period as well. After 30 May until recovery of the station, both pitch and roll angles fluctuated greatly. The cause of this instability might have been substantial damage to the station's feet. In fact, at the time the station was picked up, all three feet were missing or damaged. As a result, the station had become unstable and it only remained upright because of the buoyancy of the glass spheres mounted on the top of the frame.
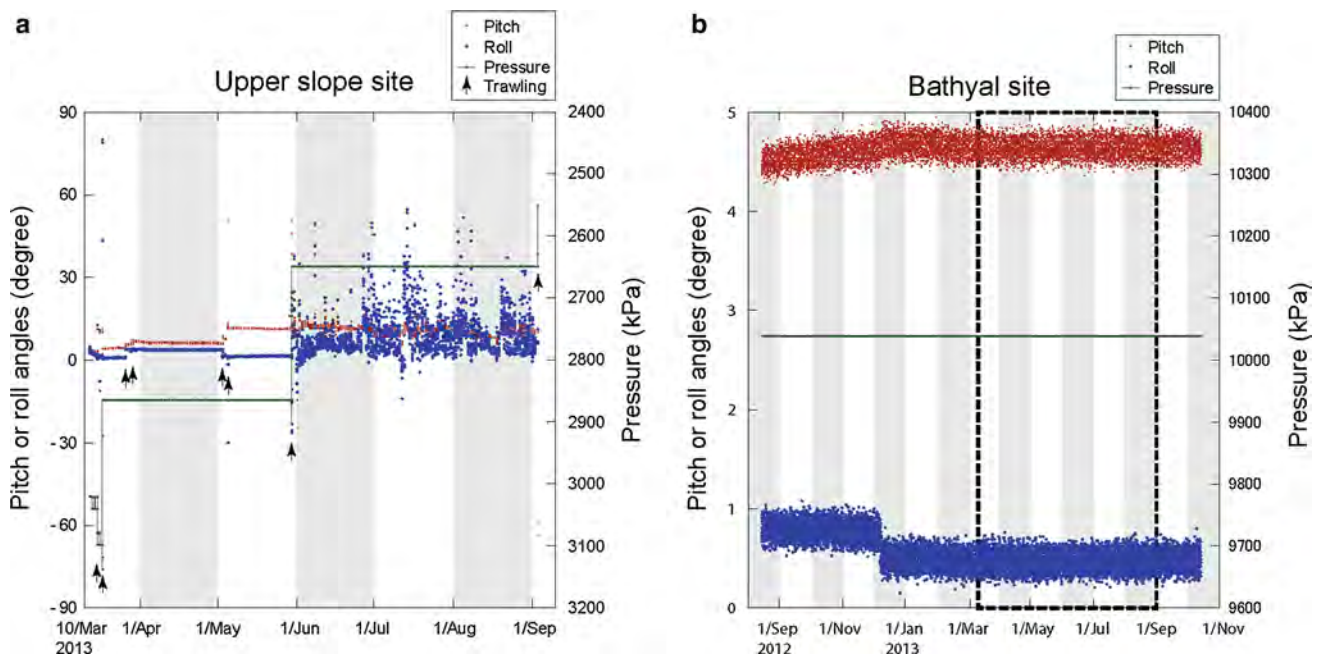
Fig. 3 Temporal changes in pitch (*red dots*) and roll (*blue dots*) angles and hydrostatic pressure (*green dots* and *line*) at the **a** upper slope and **b** bathyal sites. *Arrows* **a** indicate times when the hydrostatic pressure and azimuth sensor data suggest movement of the station cause by trawling. The *dashed box* in **b** shows the period of station deployment at the upper slope site

3.3 Hydrostatic pressure and pitch and roll at the bathyal site

At the bathyal site, hydrostatic pressure and the pitch and roll angles were stable throughout the deployment, except for a small increase of the roll angle at 17:38 on 7 December 2012. After that time, the station was tilted eastward from $0.77° ± 0.09°$ to $0.51° ± 0.10°$. At the same time, the pitch angle, which showed a weak increasing trend before this time, ceased increasing (Fig. 3b). These changes occurred shortly after a strong earthquake (17:18 JST on 7 December; $M = 7.3$; hypocenter, 38°1.1′N, 143°52.0′E at 49 km depth below the seafloor; Japan Meteorological Agency 2015). The hypocenter location indicated that this event was an aftershock of the 2011 Tohoku Earthquake. Even though the mainshock had occurred 21 months before, seismic activity in this area was still high. The seismic shaking at the bathyal site would have been severe, considering the magnitude of the earthquake, the distance between the bathyal site and the epicenter (190 km southeast of the bathyal site), and the observed change in the tilt angle of the station. This earthquake generated a weak tsunami along the northeast coast (Japan Meteorological Agency 2012), but a distinct pressure change was not recorded by our pressure sensor. The effect of this remarkable event on the seafloor and its benthic habitats is discussed in Sect. 4.

3.4 Current velocity and direction at the upper slope site

Although the RDCP 600 automatically compensated the current velocity and direction when the tilt angle was smaller than $±20°$ (Aanderaa Data Instruments 2006), we found notable tilt anomalies exceeding $±20°$ after 30 May. Therefore, we excluded current velocity and direction data accompanied by pitch and roll angles larger than $±20°$ from the analysis. The 25-h averaged current velocity ranged from 0 to 32 cm s^{-1}, and the dominant current direction was from NNE to SSW, or, occasionally, from S–SSW to N–NNE (Fig. 4a). These directions are parallel to the isobaths of the bottom topography.

3.5 Current velocity and direction at bathyal site

At the bathyal site, the 25-h averaged current velocity ranged from 2 to 23 cm s^{-1}. There were two dominant current directions: from NNW to SSE and from SW to NE (Fig. 4b). As at the upper slope site, the current direction seemed to be parallel to the bottom topography isobaths.

3.6 Temperature, salinity, and DO at the upper slope site

During the deployment, the bottom temperature varied considerably between 1.8 and 8.1 °C (Fig. 5a). After a
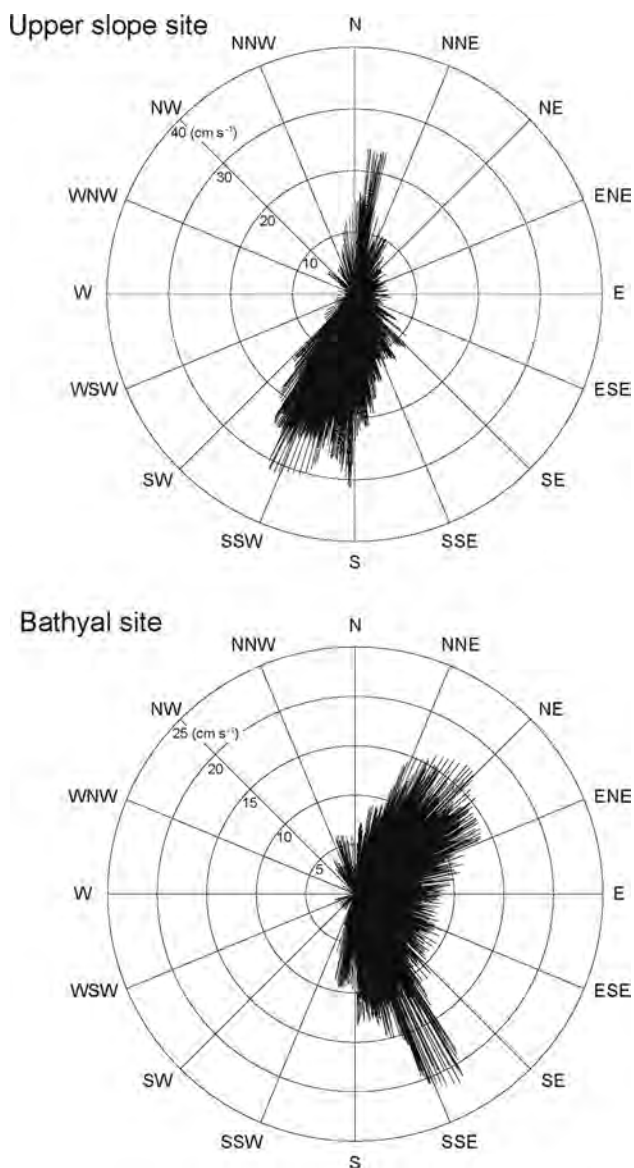
Fig. 4 Compass plots of current intensity and velocity observed at the upper slope (*top*) and bathyal (*bottom*) sites, measured 5.5 m above the seafloor

marked decrease between 2 and 10 May, the temperature showed a generally increasing trend until mid-July but remained lower than temperatures recorded before early May. Salinity changes seemed to correlate with the temperature (Fig. 5b); a notable decrease from 34.01 to 33.33 was recorded between 4 and 9 May, and brief spikes were observed throughout the monitoring period. The DO concentration was relatively high, at 250–320 μM, throughout the observation period, and there was no distinct seasonal trend. Brief falls in DO to below 250 μM were observed throughout the deployment (Fig. 5c).

3.7 Temperature, salinity, and DO at the bathyal site

Temperature at bathyal site was quite stable, averaging 2.91 ± 0.12 °C throughout the observation period, without any distinct fluctuations (Fig. 5d). Salinity fluctuation was also small; the average salinity was 34.41 ± 0.11 (Fig. 5e). The water mass at the site was typical intermediate water, which is characterized as cold lower water system defined by Hanawa and Mitsudera (1986). From early March to mid-August 2013, salinity tended to decrease. This period coincides with the period of strong temperature and salinity decreases at the upper slope site. The average DO during the deployment of 24.7 ± 2.2 μM (Fig. 5f) is representative of depleted O_2 values found in intermediate waters of the northwest Pacific (Ogura 1970; Nomaki et al. 2015), and DO did not fluctuate seasonally.

3.8 Turbidity at the upper slope site

Turbidity at the upper slope site was less than 0.1 NTU except during March to May and July 2013 (Fig. 5g). The turbidity increase was particularly distinct in spring. Brief spikes to values exceeding 10 NTU were observed on 17 and 24 March and on 16 April. The peak on 17 March may have resulted from a disturbance caused by trawling, because the roll and pitch angles also fluctuated markedly on that date. However, similar artifacts did not accompany the other turbidity spikes. Remarkably, the high turbidity recorded on 16 April exceeded the maximum sensor reading of 25 NTU. We discuss the relationships among turbidity, marine snowfall, and the chlorophyll *a* concentration at the sea surface in Sect. 4.

3.9 Turbidity at the bathyal site

At the bathyal site, turbidity was stable, typically 0.4 NTU, until mid-January 2013 (Fig. 5h), and slightly higher than turbidity at the upper slope site. After mid-January 2013, turbidity gradually increased with frequent spikes. The photographs did not confirm this increasing trend at the seafloor, though they showed sporadic turbidity increases and decreases. Therefore, we assumed that the data do not reflect the true turbidity. Because both cameras captured images of unidentified organisms and organic material, we interpret these elevated turbidities to reflect, for example, biofouling of the photosensor.

3.10 Sediment characteristics and the benthos at the upper slope site

Fine-grained sand particles are dominant on the seafloor at around 300 m water depth off Otsuchi Bay (Arita and

Fig. 5 **a** Temperature, **b** salinity, and **c** DO observed at the upper slope site. **d** Temperature, **e** salinity, and **f** DO observed at the bathyal site. **g**, **h** Turbidity observed at the upper slope and bathyal sites. The *dashed boxes* in the bathyal site graphs show the observation period at the upper slope site. *Gray lines* in (**g**, **h**) indicate period of high (>0.5 mg m^{-3}) chlorophyll *a* concentrations at the sea surface, observed by satellite remote sensing. *Small arrows* in (**g**) indicate movement of the station inferred from the hydrostatic pressure and azimuth sensor data. The *large arrow* in (**h**) indicates the occurrence time of the earthquake (see text)
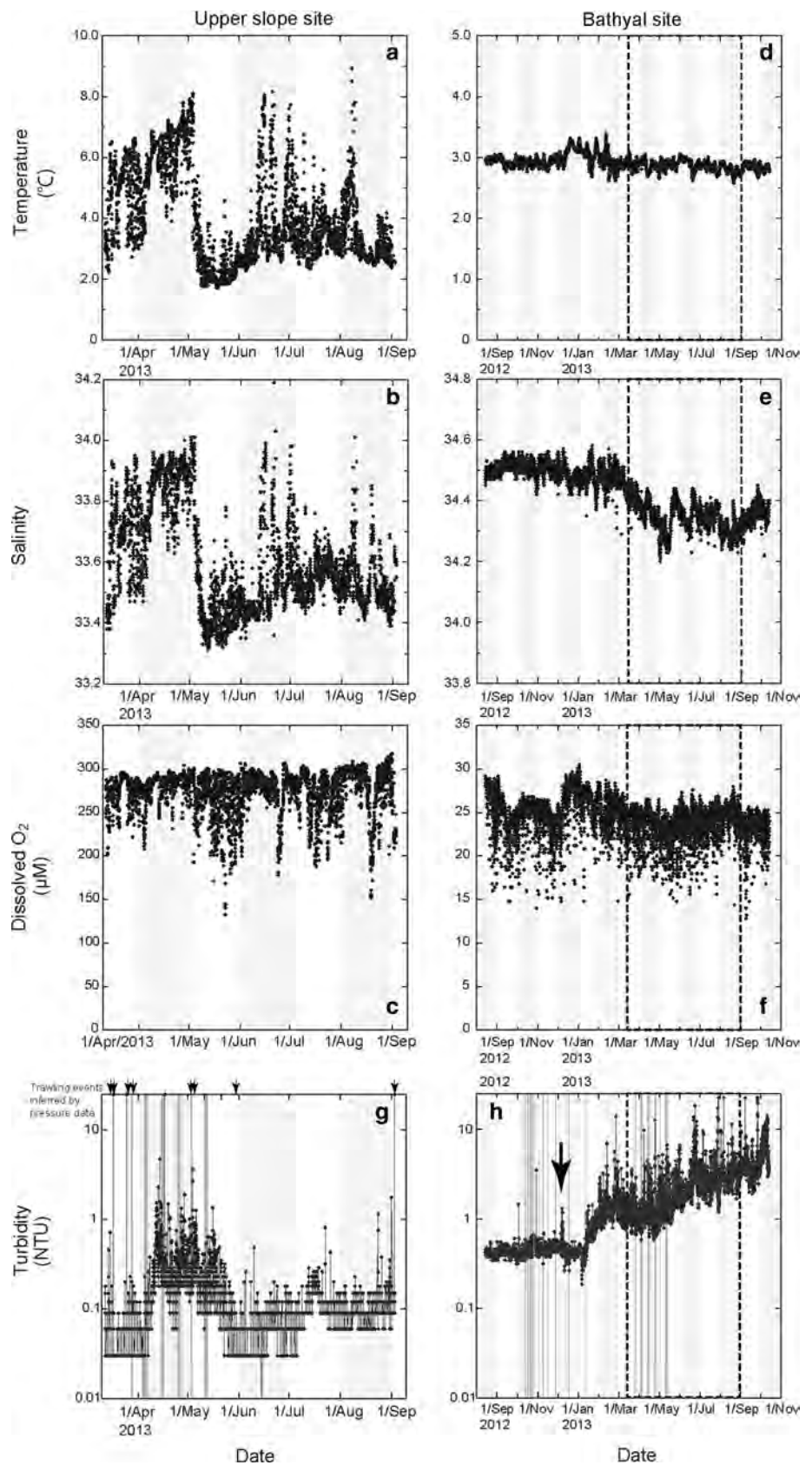
Fig. 6 Seafloor photographs taken by the camera at the upper slope ▶ site. The photographs show a trapezoidal area of seafloor 115 cm (transversal direction) by 50 cm. **a** Ophiuroid communities cover the seafloor. **b**, **c** Marine snowfall observed following spring phytoplankton blooms. **c** Photograph of the highest density marine snowfall during the deployment period. The seafloor is completely hidden. **d** The seafloor after the spring phytoplankton blooms. Ophiuroids are absent around the sea anemone, seen in the center of the photograph

Kinoshita 1984), and the seafloor photographs that we obtained show sediment characteristics consistent with those results. The sediment surface was homogenous; no pebbles or other coarse particles were seen, and *Ophiura sarsii* were distributed densely on the seafloor (Fig. 6). Similar high ophiuroid densities have been reported previously (Fujita and Ohta 1989). No disturbance effect from the 2011 Tohoku Earthquake was apparent in the photographs. The ophiuroid population seemed stable throughout the observation period, and individuals tended to stay in the same place for several days or move only small distances. The density, size distribution, and seasonal fluctuations of the ophiuroids have been analyzed by Yamakita et al. (personal communication). In addition, unidentified species of gastropods, sea anemones, and paguroidea appeared in the photographs. One sea anemone remained at the same spot in front of the station from 31 March to 30 May, and ophiuroids tended to avoid the area around the anemone. Cod fish (*Theragra chalcogramma* and *Gadus macrocephalus*) also appeared in the photographs. All the photographs are combined as Supplementary video 1.

3.11 Sediment characteristics and the benthos at the bathyal site

At water depths deeper than 800 m off Otsuchi Bay, sediment particles are dominantly silt-sized (Arita and Kinoshita 1984), although in the photographs, it was hard to tell grain size, muddy sediment covers the seafloor homogeneously, and many holes, possibly dug by benthic organisms, were observed. In the time-lapse photographs, ophiuroids sometimes appeared to hide in these holes (Fig. 7). The dominant benthic organism was an unidentified ophiuroid. Unlike *Ophiura sarsii* at the upper slope site, the ophiuroids at the bathyal site were smaller and their density was much lower. However, they moved actively about the seafloor. Trails made by benthic organisms, perhaps gastropods or sea cucumbers, remained on the seafloor for up to 1 week. Fish appearing in the photographs were deep-sea eels (unidentified species), *Coryphaenoides* sp., and *Sebastolobus macrochir*. All the photographs are combined as Supplementary video 2.
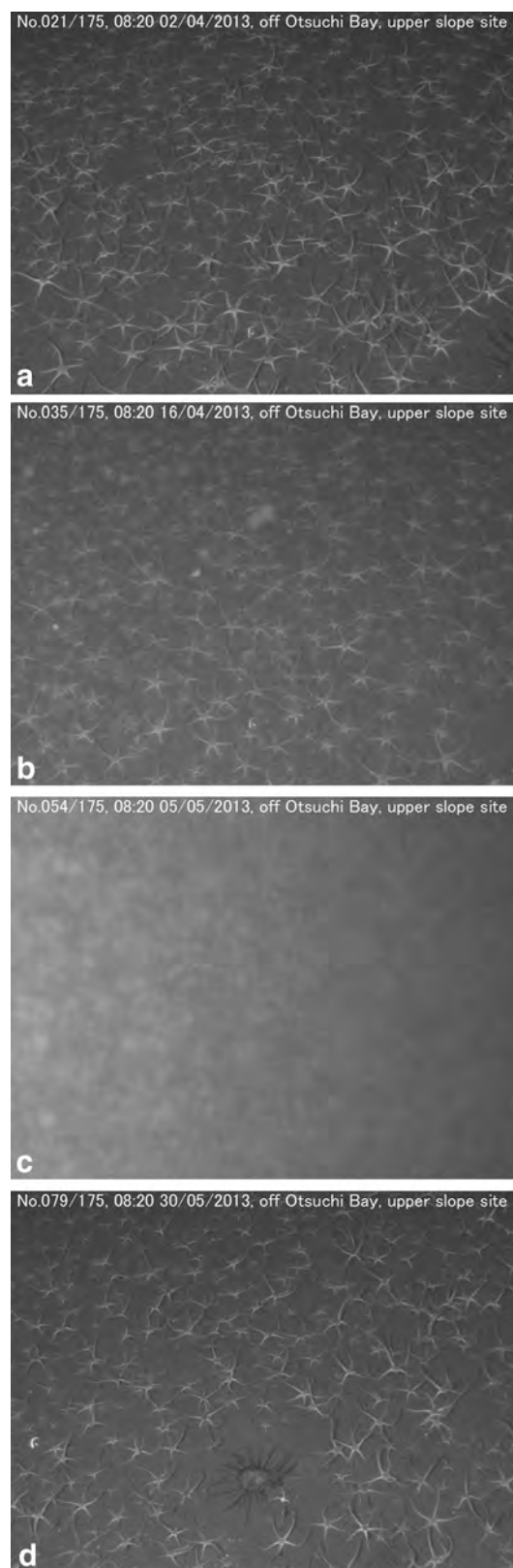
Fig. 7 Seafloor photographs taken by the camera at the bathyal site. The photographs show a trapezoidal area of seafloor 115 cm (transversal direction) by 50 cm. **a** Typical view of the seafloor showing small ophiuroids. **b** A frame with a *Sebastolobus macrochir* individual. **c** Marine snowfall observed in late winter. The dense marine snow obscures the seafloor

4 Discussion

4.1 Long-term drift of the O_2 sensor at the upper slope site

DO values at the upper slope site drifted downward during the monitoring period. Although the optical O_2 (optode) sensor used has more long-term stability than conventional electrode-based sensors (Tengberg et al. 2003, 2006), changes in sensor performance can be considerable. For example, photobleaching of the O_2 sensitive dye and membrane, which is enhanced at higher O_2 concentrations,

decreases the intensity and lifetime of the luminescent dye (Hartmann et al. 1998). However, because these effects are inversely proportional to the O_2 concentration (Kautsky 1939), photobleaching should increase DO values. Therefore, photobleaching cannot account for the DO drift. Another possible causes are enhanced O_2 consumption caused by fouling of organisms including microbial mats on the sensor foil, or ageing of the electronics. By naked eye observations, significant biofouling which was often seen after shallow water deployments (e.g., Martini et al. 2007) was not identified on the sensor foil after the recovery of the station and a biofouling effect cannot reasonably be inferred. Considerable ageing of the electronic components used in the circuit occurred, though it is difficult to find direct evidence of an ageing effect. We estimated the degradation rate by subtracting atmospheric O_2 values obtained before the deployment from those obtained after the deployment and assuming a constant rate of degradation.

4.2 Cause of the increasing turbidity at the bathyal site

At the bathyal site, the sensor indicated that turbidity increased after mid-January 2013 (Fig. 5h), but this increasing turbidity was not apparent in the time-lapse photographs (Supplementary video 2); thus, the increase did not seem to reflect a true change in turbidity. At both sites, organisms were observed near or on the camera window in the photographs. Therefore, biofouling of the turbidity sensor surface may account for the observed increase. Although no prominent turbidity increase was recorded at the upper slope site, unidentified anthozoan organisms can be seen in the photographs taken on 10, 12, 16, 26, and 27 May and between 5 and 13 June 2013 (Supplementary video 1). Such organisms remaining on or close to the turbidity sensor for a long time would interfere with the turbidity measurement. Similarly, at the bathyal site, small unidentified organisms often appeared in the camera window from 29 July to 23 September 2013. Even after they could no longer be seen in the photographs, adhesive material remained on the camera window (Supplementary video 2). In any case, only the DO and turbidity sensors are sensitive to fouling effects, and we assumed that chance interference by organisms affected the readings of these sensors during the monitoring period. Organisms and organic matter are likely to be removed by wave action during recovery of the stations, so direct evidence of biofouling would not necessarily be observed after their recovery.

4.3 Short-term fluctuations of current velocity and temperature at the upper slope site

At the upper slope site, many brief temperature spikes with amplitudes of from 2 to 6–8 °C were recorded. Fast Fourier

Fig. 8 Results of FFT analyses of **a** the NS and EW components of current velocity and **b** water temperature at the upper slope site
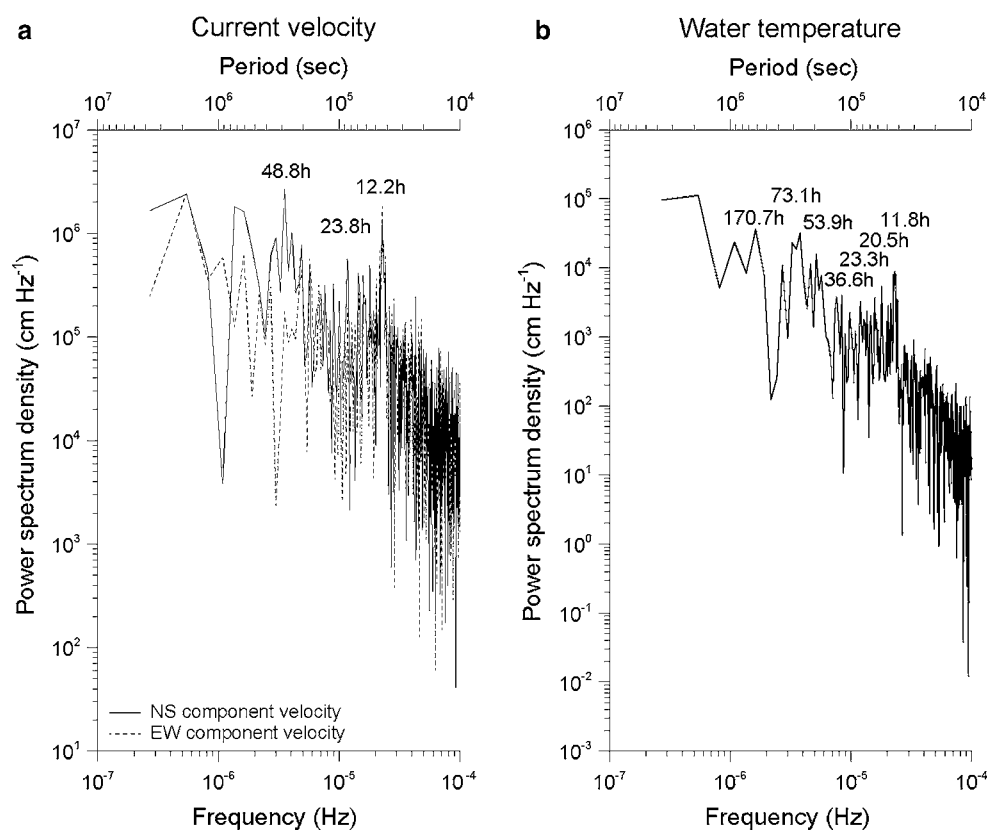
Transform (FFT) analysis of the NS and EW components of current velocity and of temperature indicated the existence of current velocity cycles with periods of 12.2, 23.8 (both NS and EW components), and 48.8 h (NS component) hours (Fig. 8a). The 12.2 h cycle relates to the M2 (principal lunar) harmonic, and the 23.8 h cycle corresponds to the K1 (luni-solar diurnal) harmonic. Therefore, the current velocity fluctuations apparently reflect tidal cycles. Temperature fluctuated with cycles of 11.8, 20.5, 23.3, 36.6, 53.9, 73.1, and 170.7 h (Fig. 8b). Although most of these cycles are longer than the tidal cycles, the 11.8 and 23.3 h cycles are close to the K2 (luni-solar declinational) and K1 harmonics, respectively. Therefore, the causes of the temperature variation are unknown, though K2 and K1 harmonics might have influenced the temperature fluctuations.

4.4 Water mass changes at the upper slope site

Water temperature and salinity at the upper slope site decreased significantly in May 2013 (Figs. 5a, b), apparently as a result of a seasonal water mass change. The temperature–salinity diagram, in which data from the stations as well as the CTD data obtained during the BO13-20 cruise were compared with water masses in the region (Fig. 9a), indicates that water masses of three origins (Hanawa and

Mitsudera 1986): Tsugaru warm current water, characterized by relatively higher temperatures (>5 °C) and salinity between 33.7 and 34.2; Oyashio water, characterized by lower temperatures (0–7 °C) and salinity between 33.0 and 33.7 at densities of $\sigma_t \leq 26.7$; and a cold, lower level water mass, characterized by lower temperatures and salinity larger than 33.3 at densities $\sigma_t \geq 26.7$. The Tsugaru warm current, which flows from the Japan Sea out to the Pacific through the Tsugaru Strait, originates from the Tsushima warm current, which branches off from the Kuroshio current in the East China Sea (e.g., Yasuda 2003). In contrast, the Oyashio water system is derived from the Oyashio cold current in the North Pacific and Okhotsk Sea, which flows along the Kuril Islands and off southeastern Hokkaido (e.g., Yasuda 2003). The characteristics of the cold lower level water are typical of North Pacific Intermediate Water, which forms by the mixing of Kuroshio and Oyashio waters (Talley et al. 1995; Shimizu et al. 2004). Thus, in early May, Tsugaru warm current water was exchanged for Oyashio water system water (Fig. 9a). This water mass exchange is also supported simulation results obtained by the Japan Meteorological Agency (JMA) by using a global circulation model with data assimilation (http://www.data.jma.go.jp/kaiyou/data/db/kaikyo/jun/t100_HQ.html?areano=1; accessed on 7 September 2015). In addition, Oguma et al. (2002) analyzed the seasonal distributions of water masses off Sanriku using data obtained
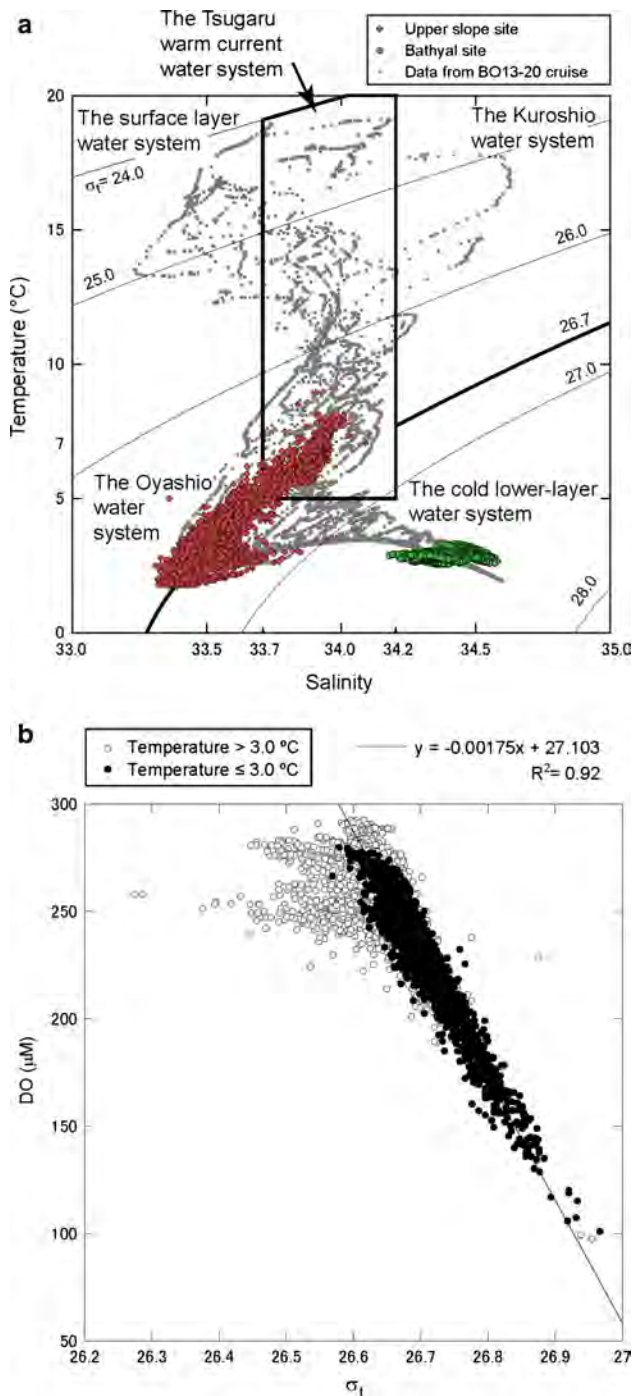
Fig. 9 a Temperature–salinity data from the upper slope (*red diamonds*) and bathyal sites (*green circles*) and from the CTD profiles obtained during the BO13-20 cruise (*gray dots*). Typical water mass end-member distribution patterns are defined by Hanawa and Mitsuzawa (1986). **b** Plot of DO versus density (σ_t) at the upper slope site. The *solid line* was fitted by the least-squares method to DO (*y*-axis) and σ_t (*x*-axis) data for temperatures ≤3.0 °C

from 1971 to 1995 and concluded that Tsugaru warm water was dominant in the region from January to April, whereas in late May the front between Tsugaru warm water and

Oyashio water formed in the area. Our inference regarding a seasonal water mass exchange at the upper slope site is therefore consistent with both the JMA modeling results and the observational evidence reported by Oguma et al. (2002).

At the upper slope site, frequent, sporadic DO decreases were observed (Fig. 5c). Remarkably, from 24 to 26 June 2013 and from 18 to 21 August 2013, DO decreased to less than 250 μM for relatively long periods. Minima were recorded on 24 June (178 μM) and on 19 August (152 μM). Because the DO shows a decreasing trend from the sea surface to 1000 m depth in the area off Sanriku (Ogura 1970; Fontanier et al. 2014; Nomaki et al. 2015), we inferred that the DO decreases that we observed were caused by intermittent upwelling of deeper water. During the periods when DO was low, σ_t was increased. A scatter plot of DO against σ_t showed a good correlation between σ_t and DO when the water temperature was ≤3.0 °C (Fig. 9b). This result is consistent with the occurrence of upwelling at the upper slope site, but the mechanism of the upwelling cannot be determined from our data. If such upwelling is occurred, increase of chlorophyll *a* concentration can be confirmed by satellite remote sensing, because deeper seawater contains higher nutrients and it stimulates phytoplankton growth (e.g., Saitoh et al. 1998). We could not confirm that increase in the chlorophyll *a* concentration in the surface seawater coincided with these DO fluctuations because remote sensing data for these periods are not available. The relationships between these events and the migration of organisms, from phytoplankton to fish, should be investigated by further multidisciplinary monitoring and observations.

4.5 Temporal and spatial fluctuations in marine snow

The high turbidity spikes exceeding 1 NTU recorded by the turbidity sensors at both sites lasted only from 1 to several hours. Satellite observations showed chlorophyll *a* concentrations exceeding 0.5 mg m^{-3} in the surface seawater from 4 to 5, 14 to 15, and 23 to 25 April 2013 (NASA AQUA satellite and analyses by Earth Observation Research Center, Japan Aerospace Exploration Agency, and Tokai University). The processed images are available at the MODIS near real time data site: http://kuroshio.eorc.jaxa.jp/ADEOS/mod_nrt_new/index.html (accessed on 7 September 2015). Another prominent chlorophyll *a* increase was observed around 2 and 8–10 May 2013. The camera at the upper slope site also recorded high levels of marine snow on 5 May (Fig. 6). Therefore, we attributed the sporadic turbidity increases to dense marine snowfall related to phytoplankton blooms at the sea surface. Saino et al. (1998) reported short-term spikes in the organic carbon flux in sediment traps deployed off Sanriku. Our turbidity sensor data and photographic evidence support their finding,

namely, that heavy short-term marine snowfalls transport substantial amounts of organic carbon to the seafloor in this area.

Before the beginning of the marked turbidity drift at the bathyal site, two turbidity spikes were observed, on 2 and 30 October 2012. These peaks may correspond to the broad phytoplankton blooms observed from mid- to late October (MODIS near-real-time data), when the sinking speed of biogenic organic materials of 90–200 m day^{-1} is taken into account (Buesseler et al. 1990; Deuser et al. 1990; Honda et al. 2012, 2013). A photograph taken on 2 February 2013 (Fig. 7) also shows considerable marine snow. Prior to this snowfall event, from 20 to 23 January 2013, high chlorophyll *a* concentrations were observed in the surface seawater (MODIS near-real-time data). Using these observation results, we estimated the sinking speed of the marine snow to be 77–100 m day^{-1}, which is similar to the previously reported values. In addition to the turbidity peaks by marine snowfall, another prominent turbidity increase was observed on 7 December 2012. This increase was not preceded by a distinct chlorophyll *a* increase at the sea surface, and no artificial disturbance was recorded from the hydrostatic pressure and the tilt angle. A possible cause is the earthquake that occurred on this date.

4.6 Effect of the earthquake on the seafloor environment

An unusual sedimentation event was recorded at the bathyal site during the observation period. An earthquake occurred at 17:18 JST on 7 December 2012, and shortly thereafter, at 22:59 on 7 December, the turbidity increased to 1.29 NTU. By 12:59 on 8 December, however, the turbidity decreased to the level before the earthquake (Fig. 10b). Before and during this event, the horizontal and vertical current velocities showed small increases (Fig. 10a, b). In a photograph taken before the event, many ophiuroids and some holes could be seen on the seafloor (Fig. 10c), whereas in photographs taken after the earthquake, a thin accumulation of sediment particles could be seen on the surface of the seafloor (Figs. 10d, e). In particular, in the photograph taken 6 h 40 min after the earthquake, at 23:58 on 7 December, the bottom water was turbid and the ophiuroids were buried in sediment (Fig. 10d). By 23:58 on 8 December, however, turbidity was no longer increasing and ophiuroids were again visible on the seafloor (Fig. 10e). Although it is hard to estimate the thickness of the sediment layer deposited on the seafloor during this event from the photograph, several holes visible on the surface before the earthquake were filled with sediment. It is remarkable that the ophiuroids were able to survive and recover from the disturbance

Fig. 10 Temporal changes in **a** vertical current velocity and **b** horizontal current intensity, direction, turbidity (*blue dots*) and temperature (*red dots*) at the bathyal site around the time of the earthquake. Photographs of the seafloor: **c** before the earthquake; **d** 6 h and 20 min after the earthquake, showing a distinct turbidity increase in the latter with ophiuroids buried in the sediment; **e** 1 day 6 h and 20 min after the earthquake—turbidity has decreased, and ophiuroids have returned to the sediment surface, but the holes seen before earthquake are still filled with sediment; and **f** 11 days 6 h and 20 min after the earthquake. The seafloor area shown in (**c**–**f**) is 115 cm (transversally) by 50 cm

caused by this unusual sediment deposition. The photographic evidence suggests that the holes are maintained by ophiuroid activity (supplementary video 2), and by around 10 days after the sediment deposition, the accumulated sediment had been removed from the holes (Fig. 10f).

Turbidity currents induced by earthquakes have been observed previously by cabled observatories. Mikada et al. (2006) reported that a turbidity current occurred just after the 2003 Tokachi-oki earthquake ($M = 8.0$). A deep-sea observatory at 2540 m water depth 25.5 km southeast of the epicenter recorded a hydrodynamic current velocity exceeding 100 cm s^{-1}. At the same time, temperature increased by 0.5 °C and salinity decreased by 0.2 (Mikada et al. 2006). Unfortunately, no cameras were installed in the station and no information on benthic disturbances is available. Kasaya et al. (2009) reported on a turbidity current observed by the Hatsushima deep-sea observatory (Momma et al. 1998) in Sagami Bay. Just 5 min after an earthquake, which occurred at 11:50:39 on 21 April 2006 ($M = 5.4$; epicenter, 34°56.4′N, 139°11.7′E; hypocentral depth, 7 km), an observatory very close to the epicenter (at 35°0.31′N, 139°22.5′E; 1175 m water depth) recorded a dense turbidity current by videocamera. The turbidity current dimmed the illumination for the video recording, and the transmission did not return to the level before earthquake for over 3 h. An increase in the water temperature of 0.6 °C was also recorded. Both these events were associated with a strong downslope current that lasted for a few hours. In contrast, the disturbance we recorded was not associated with any increase in either vertical or horizontal current velocities (Fig. 10a, b). In our record, a 0.2 °C decrease of temperature was observed between the 7 and 9 December 2012 (Fig. 10b). The cause of the fluctuations is, however, difficult to relate to the disturbance triggered by the earthquake, because such temperature fluctuations were often observed throughout the deployment (Fig. 5b). From these results, we estimated that turbidity current accompanied with strong light attenuation and prominent temperature increases was not induced by the 7 December 2012 event affected our site, even though turbidity increased and the holes in the seafloor were filled with sediment.
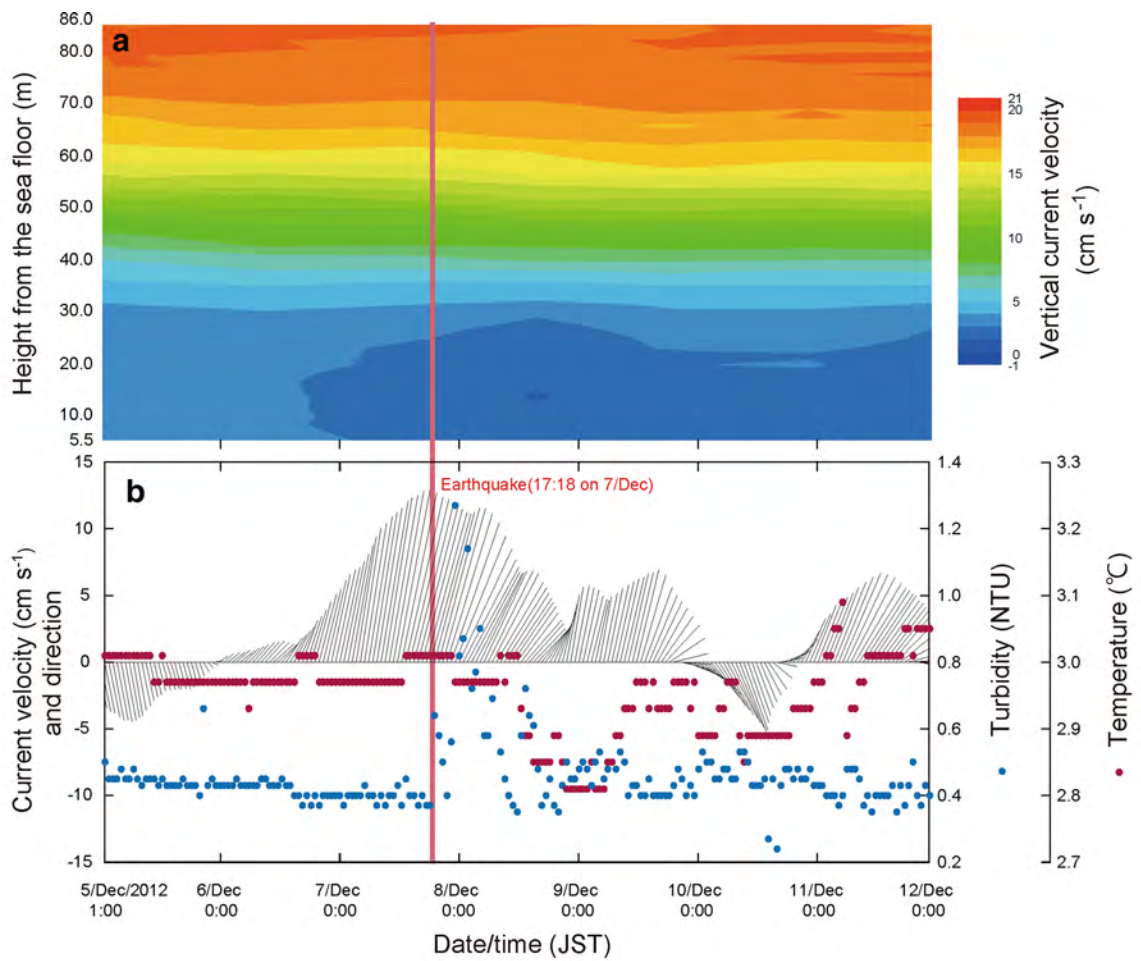
4.7 Toward wide area observations for investigating the effect of sedimentation events

We performed long-term monitoring at the two sites and they provided basic oceanographic data. However, we experienced capture of the station by trawling at the upper slope site. To minimize the risk for such accidents and in order not to bother fishery activities, monitoring sites should be carefully determined based on information from fishery communities. If possible, target sites should be shifted from trawling areas. Designing of an anti-trawling frame is also an important point. Anti-trawling ADCP frames shaped as a polygonal pyramid are commercially available from several ADCP manufacturers, and should be considered for use as a monitoring station frame for the installation of additional equipment such as batteroesy or cameraa, as well as for the recovery procedure.

The data we obtained showed the seasonal water mass exchange, occasional dense marine snowfall events associated with phytoplankton blooms, and, using the images taken by the cameras, the characteristics of the benthic habitats in the different environments. Notably, this study documented the resuspension of sediment particles and burial of benthic habitats caused by the earthquake with its magnitude of 7.3, and their subsequent recovery. Long-term monitoring has provided important knowledge of surface sediments on the seafloor since the first deep-sea observation (Lampitt 1985). Camera observations at a monitoring station can be effectively investigate an area of only several square meters. Because environmental changes at the seafloor associated with seasonal phytoplankton blooms and disturbances by earthquakes can affect wide areas with high spatial and temporal variations, monitoring should be combined with observations obtained by conventional or new technologies to better understand how seafloor environments respond to various events. Conventional surface sediment sampling, ROV, and deep-tow observations in different seasons and years are important for observing spatial seafloor variations. The use of stereo cameras with these observation methods would allow the distribution, size and mass of the benthos to be estimated (e.g., Shortis et al. 2009) and sediment surface structures to be determined. Development of a compact deep-sea HDTV video camera system that could be installed on a multiple core sampler would improve descriptions of the seafloor and benthic habitat characteristics when the sediment sampling was carried out (Toyofuku et al. 2014). Recent advances in technologies will expand our opportunities for observing the seafloor, as instruments become more compact and versatile, and less expensive. High-quality seafloor observations have the potential to make important contributions to sedimentological and oceanographic studies.

5 Conclusions

Through long-term monitoring of physical, chemical parameters and sedimentological features at different water depths off Otsuchi Bay, we were able to infer the seasonal water mass exchange and sporadic upwelling events from DO and σ_t data. The effect of tides on fluctuations of current velocity components and temperature was also investigated. Time-lapse photographs allowed us to observe benthic habitats on the seafloor and intensified marine snowfall related to increased chlorophyll *a* concentrations at the sea surface. A sedimentation event triggered by an aftershock of the 2011 Tohoku Earthquake was also documented by the turbidity sensor data and photographic evidence. The use of deep-sea stations to explore deep-sea environments is still limited. However, long-term monitoring by stations can provide valuable data of a sort that is hard to obtain from only shipboard observations. We expect that deep-sea stations that are more compact and easier to handle will be developed in the near future, and long-term monitoring, together with wide-area data obtained by conventional ships, ROVs, and deep-tow observations will shed light on many oceanographic, biological, and sedimentological phenomena on the seafloor.

References

Aanderaa Data Instruments (2003) TD 218 Operating manual Oxygen Optode 3830 and 3930. Nesttun, Norway **46**

Aanderaa Data Instruments (2006) TD 220a deployment guide recording Doppler current profiler RDCP600. Nesttun, Norway **74**

Arai K, Naruse H, Miura R, Kawamura K, Hino R, Ito Y, Inazu D, Yokokawa M, Izumi N, Murayama M, Kasaya T (2013) Tsunami-generated turbidity current of the 2011 Tohoku-Oki earthquake. Geol. doi:10.1130/G34777.1

Arita M, Kinoshita Y (1984) Sedimentological map of off Kamaishi. Geological Survey of Japan ed. Mar geol map ser 25 (**in Japanese**)

Buesseler KO, Livingston HD, Honjo S, Hay BY, Konuk T, Kempe S (1990) Scavenging and particle deposition in the southwestern

Black Sea–evidence from Chernobyl radiotracers. Deep Sea Res 37(3):413–430

Deuser WG, Muller-Karger FE, Evans RH, Brown OB, Esaias WE, Feldman GC (1990) Surface-ocean color and deep-ocean carbon flux: how close a connection? Deep Sea Res 37(8):1331–1343

Fontanier C, Duros P, Toyofuku T, Oguri K, Koho KA, Buscail R, Grémare A, Radakovitch O, Defrakdre B, deNooijer LJ, Bichon S, Goubet S, Ivanovsky A, Chabaud G, Menniti C, Reichart G-J, Kitazato H (2014) Living (Stained) deep-sea foraminifera off Hachinohe (NE JAPAN, western Pacific): environmental interplay in oxygen-depleted ecosystems. J Foram Res 44(3):281–299

Fujita T, Ohta S (1989) Spatial structure within a dense bed of the brittle star *Ophiura sarsi* (Ophiuroidea: Echinodermata) in the bathyal zone off Otsuchi, Northeastern Japan. J Oceanogr 45(5):289

Geospatial Information Authority of Japan (2010) Website of geomagnetic survey. http://vldb.gsi.go.jp/sokuchi/geomag/index.html. Accessed on 7 Sept 2015 (**in Japanese**)

Hanawa K, Mitsudera H (1986) Variation of water system distribution in the Sanriku coastal area. J Oceanogr Soc Jpn 42(6):435–446

Hartmann P, Leiner MJP, Kohlbacher P (1998) Photobleaching of a ruthenium complex in polymers used for oxygen optodes and its inhibition by singlet oxygen quenchers. Sens Actuat B 51:196–222

Hattori T, Narimatsu Y, Ito M, Ueda Y, Fujiwaram K, Kitagawa D (2007) Growth changes in bighead thornyhead *Sebastolobus macrochir* off the Pacific coast of northern Honshu, Japan. Fish Sci 73:341–347

Honda MC, Aono T, Aoyama M, Hamajima Y, Kawakami H, Kitamura M, Masumoto Y, Miyazawa Y, Takigawa M, Saino T (2012) Dispersion of artificial caesium-134 and -137 in the western North Pacific one month after the Fukushima accident. Geochem J 46:e1–e9

Honda MC, Kawakami H, Watanabe S, Saino T (2013) Concentration and vertical flux of Fukushima-derived radiocesium in sinking particles from two sites in the Northwestern Pacific Ocean. Biogeosciences 10:3525–3534. doi:10.5194/bg-10-3525-2013

Ikehara K (2012) Offshore earthquake- and/or tsunami-induced sediment transports and their deposits: importance of marine sediment study for understanding past earthquake and tsunami. J Sedimentol Soc Japan 71:141–147 (**in Japanese with English abstract**)

Ikehara K, Usami K, Jenkins R, Ashi J, Irino T (2012) The 2011 off the Pacific coast of Tohoku earthquake and tsunami event deposits found in off Sanriku surface sediments. GSJ Interim Report, Annual Report of Investigations on Geology and Active Faults in the Coastal Zone of Japan (FY2011) 59: 37–42 (**in Japanese with English abstract**)

Iwate prefecture (2011) Annual statistical report of Iwate prefecture. http://www3.pref.iwate.jp/webdb/view/outside/s14Tokei/nenkan.html. Accessed on 7 Sept 2015 (**in Japanese**)

Japan Meteorological Agency (2012) 67th report of the 2011 Tohoku-Oki earthquake –about Sanriku-Oki earthquake occurred at 17:18 on 7th Dec. 2012. http://www.jma.go.jp/jma/press/1212/07b/201212072000.html. Accessed on 7 Sept 2015 (**in Japanese**)

Japan Meteorological Agency (2015) The seismological bulletin of Japan. http://www.data.jma.go.jp/svd/eqev/data/bulletin/index_e.html. Accessed on 21 July 2015

Kasaya T, Mitsuzawa K, Goto T, Iwase R, Sayanagi K, Araki E, Asakawa K, Mikada H, Watanabe T, Takahashi I, Nagao T (2009) Trial of multidisciplinary observation at an expandable sub-marine cabled station "Off-Hatsushima Island Observatory" in Sagami Bay. Japan Sens 9(11):9241–9254

Kautsky H (1939) Quenching of luminescence by oxygen. Trans Faraday Soc 35:216–219

Kawagucci S, Yoshida YT, Noguchi T, Honda MC, Uchida H, Ishibashi H, Nakagawa F, Tsunogai U, Okamura K, Takaki Y, Nunoura T, Miyazaki J, Hirai M, Kitazato H, Takai K (2012) Disturbance of deep-sea environments induced by the M9.0 Tohoku earthquake. Sci Rep 2. doi:10.1038/srep00270

Lampitt RS (1985) Evidence for the seasonal deposition of detritus to the deep-sea floor and its subsequent resuspension. Deep Sea Res 32(8):887–897

Martini M, Butman B, Mickelson MJ (2007) Long-term performance of aanderaa optodes and sea-bird SBE-43 dissolved-oxygen sensors bottom mounted at 32 m in Massachusetts Bay. J Atmos Ocean Tech 24:1924–1935

Mikada H, Mitsuzawa K, Matsumoto H, Watanabe T, Morita S, Otsuka R, Sugioka H, Baba T, Araki E, Suyehiro K (2006) New discoveries in dynamics of an M8 earthquake-phenomena and their implications from the 2003 Tokachi-oki earthquake using a long term monitoring cabled observatory. Tectonophys 426(1–2):95–105

Momma H, Iwase R, Mitsuzawa K, Kaiho Y, Fujiwara Y (1998) Preliminary results of a three-year continuous observation by a deep seafloor observatory in Sagami Bay, central Japan. Phys Earth Planet Inter 108(4):263–274. doi:10.1016/S0031-9201(98)00107-1

Noguchi T, Tanikawa W, Hirose T, Lin W, Kawagucci S, Yoshida YT, Honda MC, Takai K, Kitazato H, Okamura K (2012) Dynamic process of turbidity generation triggered by the 2011 Tohoku-Oki earthquake. Geochem Geophys Geosys 13:Q11003. doi:10.1029/2012GC004360

Nomaki H, Arai K, Suga H, Toyofuku T, Wakita M, Nunoura T, Oguri K, Kasaya T, Watanabe S (2015) Sedimentary organic matter contents and porewater chemistry at upper bathyal depths influenced by the 2011 off the Pacific coast of Tohoku Earthquake and tsunami. J Oceanogr. doi:10.1007/s10872-015-0315-3 (in press)

Oguma S, Suzuki Y, Nagata Y (2002) Seasonal variations in the sea off Sanriku Coast, Japan. J Oceanogr 58:825–835

Ogura N (1970) The relation between dissolved organic carbon and apparent oxygen utilization in the Western North Pacific. Deep Sea Res 17(2):221–231

Oguri K, Kawamura K, Sakaguchi A, Toyofuku T, Kaasaya T, Murayama M, Glud RN, Kitazato H (2013) Hadal disturbance in the Japan Trench induced by the 2011 Tohoku-Oki Earthquake. Sci Rep. doi:10.1038/srep01915

Oguri K, Yamamoto M, Toyofuku T, Kitazato H (2015) Developments of deep-sea light and charge pump circuits fixed with an epoxy resin. JAMSTEC Rep Res Dev 21:7–15 (**in Japanese with English abstract**)

Ozawa S, Nishimura T, Suito H, Kobayashi T, Tobita M, Imakiire T (2011) Coseismic and postseismic slip of the 2011 magnitude-9 Tohoku-Oki earthquake. Nature 475:373–376. doi:10.1038/nature10227

Saino T, Shang S, Mino Y, Suzuki K, Nomura H, Saitoh S, Miyake H, Masuzawa T, Harada K (1998) Short term variability of particle fluxes and its relation to variability in sea surface temperature and Chlorophyll *a* field detected by ocean color and temperature scanner (OCTS) off Sanriku, Northwestern North Pacific in the spring of 1997. J Oceanogr 54:583–592

Saitoh S, Inagake D, Sasaoka K, Ishizaka J, Nakame Y, Saino T (1998) Satellite and ship observations of Kuroshio warm-core ring 93A off Sanriku, Northwestern North Pacific, in spring 1997. J Oceanogr 54:495–508

Sakaguchi-Orui S, Takishita K, Goto T, Shibata H, Kojima S, Tsuchida S, Kitazato H, Fujikura K (2014) Analyses of age and population genetic structure of the broadbanded thornyhead *Sebastolobus macrochir* in North Japan suggest its broad

dispersion and migration before settlement. J Oceanogr 70:457–462. doi:10.1007/s10872-014-240-x

Sato M, Ishikawa T, Ujihara N, Yoshida S, Fujita M, Mochizuki M, Asada A (2011) Displacement above the hypocenter of the 2011 Tohoku-Oki earthquake. Science 332:1395. doi:10.1126/science.1207401

Shimizu Y, Iwao T, Yasuda I, Ito S, Watanabe T, Uehara K, Shikama N, Nakano Y (2004) Formation process of North Pacific Intermediate Water revealed by profiling floats set to drift on 26.7 σ_θ isopycnal surface. J Oceanogr 60:453–462

Shortis M, Harvey E, Abdo D (2009) A review of underwater stereo-image measurement for marine biology and ecology applications. Oceanogr Mar Biol Annu Rev 47:257–292

Smith KL, Clifford CH, Eliason AH, Walden B, Rowe GT, Teal JM (1976) A free vehicle for measuring benthic community metabolism. Limnol Oceanogr 21(1):164–170

Talley LD, Nagata Y, Fujimura M, Iwao T, Kono T, Inagake D, Hirai M, Okuda K (1995) North Pacific Intermediate Water in the Kuroshio/Oyashio mixed water region. J Phys Oceanogr 25:475–501

Tengberg A, DeBovee F, Hal PW, Berelson WD, Chadwick DG, Ciceri GP, Crassous PA, Devol AS, Emerson SJ, Gage JR, Glud RN, Graziottini FJ, Gundersen JD, Hammond DW, Helder WK, Hinga KO, Holby OR, Jahnke RA, Khripounoff AS, Lieberman SV, Nuppenau VO, Pfannkuche OC, Reimers CG, Rowe GA, Sahami AF, Sayles FM, Schurter MD, Smallman D, Wehrli B, DeWilde P (1995) Benthic chamber and profiling landers in oceanography—a review of design, technical solutions and functioning. Prog Oceanogr 35(3):253–294

Tengberg A, Hovdenes J, Barranger D, Brocandel O, Diaz R, Sarkkula J, Huber C, Stangelmayer A (2003) Optodes to measure oxygen in the aquatic environment. Sea Techn 44:10–15

Tengberg A, Hovdenes J, Andersson HJ, Brocandel O, Diaz R, Hebert D, Arnerich T, Huber C, Körtzinger A, Khripounoff A, Rey F, Rönning C, Schimanski J, Sommer S, Stangelmayer A (2006) Evaluation of a lifetime-based optode to measure oxygen in aquatic systems. Limnol Oceanogr Meth 4(2):7–17

Toyofuku T, Duros P, Fontanier C, Mamo B, Bichon S, Buscail R, Chabaud G, Deflandre B, Goubet S, Grémare A, Menniti C, Fujii M, Kawamura K, Annika Koho K, Noda A, Namegaya Y, Oguri K, Radakovitch O, Murayama M, deNooijer LJ, Kurasawa A, Ohkawara N, Okutani T, Sakaguchi A, Jorissen F, Reichart G-J, Kitazato H (2014) Unexpected biotic resilience on the Japanese seafloor caused by the 2011 Tōhoku-Oki tsunami. Sci Rep 4:7517. doi:10.1038/srep07517

Uchida H, Kawano T, Kaneko I, Fukasawa M (2008) In situ calibration of optode–based oxygen sensors. J Atmos Ocean Techn 25:2271–2281. doi:10.1175/2008JTECHO549.1

Yasuda I (2003) Hydrographic structure and variability in the Kuroshio-Oyashio transition area. J Oceanogr 59:389–402